Adaptive droop control design with overcurrent protection for onboard DC microgrids in hybrid electric aircrafts

Andrei-Constantin Braitor, Houria Siguerdidjane, Alessio Iovine

Adaptive droop control design with overcurrent protection for onboard DC microgrids in hybrid electric aircrafts

Andrei-Constantin Braitor, Houria Siguerdidjane, Alessio Iovine

Laboratoire des Signaux et Systèmes, CentraleSupélec, CNRS, Université Paris-Saclay, Gif-sur-Yvette, France (e-mail: {andrei.braitor,alessio.iovine,houria.siguerdidjane}@centralesupelec.fr).

Abstract: In this paper, an adaptive nonlinear droop-based control approach is proposed for converter-based self-contained electrical power systems (EPS) designed for electric aircraft applications to ensure tight voltage regulation and accurate load power distribution among parallel sources. By taking into account the accurate nonlinear dynamic models of the power converters, we mathematically prove an upper bound for the input current of each converter separately by means of Lyapunov methods and ultimate boundedness theory. In particular, the adopted nonlinear droop-based controller introduces a virtual voltage and a virtual resistance in series with the inductance and parasitic resistance of each DC/DC boost converter. To verify the proposed controller performance and its underlying developed theory, simulation results of the low-voltage bus dynamics have been presented for an onboard aicraft DC microgrid (MG).

Keywords: hybrid electric aircraft, adaptive droop control, DC microgrids.

1. INTRODUCTION

Aircraft electrical power systems are self-contained networks of energy sources that power avionics, flight controls, communications, lighting systems, and a myriad of other key functional elements. To minimise emissions, environmental impact and lifetime operational costs, all components must have high reliability, but also reduced size and weight to deliver the highest operational efficiency. This, in due course, will drive the trend towards electrifying more subsystems and put EPS at the heart of electric propulsion options in future aircraft designs, aimed to ensure uninterruptible power supply during the entire flight plan (Wheeler and Bozhko, 2014; Roboam et al., 2012).

This initiative to replace the existing hydraulic, pneumatic, and mechanical actuators with electrical systems would enable a rebalancing of energy use in the aircraft, allowing optimisation at different flight stages, and ultimately exploiting the advantages of aircraft EPS controllers. More recent models, such as Boeing 787 and the Airbus A380, have more electrical power components installed compared to older models (Gaynor, 2015; Steinbauer et al., 2004), and this trend is expected to increase further in the future. Nevertheless, scaling up the onboard installed electrical power introduces additional challenges in the design and control of the aircraft electrical network.

In this race towards electrification, DC MGs emerged as a potential solution for the distribution power system installed onboard aicrafts, given their unparalleled advantages, such as high efficiency, natural interface to battery energy storage systems (BESS), straightforward control structure, absence of reactive power and frequency, reduced DC/AC conversion stages, etc. In general, the control challenges one faces in onboard DC microgrids are related to voltage regulation, load power distribution among paralleled sources, overall stability, and system protection (Jin et al., 2022).

Onboard DC microgrids with enhanced reliability that do not use communication among the units, often operate in a distributed control manner where the control method for each unit is based on the available local variables. Droop controllers have been successfully utilised in decentralised approaches given their simplicity and linear behaviour, and without extra communication lines, thus, increasing the overall system modularity, reliability and likewise reducing costs (Guerrero et al., 2011; Braitor et al., 2018). Nevertheless, the conventional droop introduces the trade-off between the current sharing and the voltage regulation, which may become quite significant under large load demands. To address this issue, a standard way is to employ a secondary controller to restore the voltage and improve the power sharing (Liu et al., 2018). Improved and consensus-based droop methods have also been proposed in Behera et al. (2022), and Zhang et al. (2022) respectively, where either a compensation term is introduced to increase the voltage or a consensus approach is employed to guarantee power sharing. Other versions of droop-based control methods have also been developed in Huang et al. (2015); Cingoz et al. (2017); Simpson-Porco et al. (2017). Adaptive droop controllers for microgrids that incorporate BESS have been reported in Mohamed and El-Saadany (2008), or Ferahtia et al. (2022).

Apart from the need to guarantee reliable performance, the need for safe operation without additional protection hardware, such as circuit breakers and fuses, has emerged as an active research direction for some time (Baidya and Nandi, 2022). Some methods have been proposed to tackle this aspect (see Konstantopoulos and Zhong (2019)), but still remains an open research direction.

Still falling under protection aspect is the presence of constant power loads (CPLs). Aircraft EPS include tightly regulated motors and downstream converters that behave as CPLs. The challenges that constant power loads impose stem from their power conditioning at the load side. Also, given their nonlinear expression, they behave as negative impedances in small-signal analysis (Braitor et al., 2020). As a result, the existence of a steady-state behaviour is critical for a safe and reliable operation of the DC EPS. From the analytical perspective, addressing this issue is not a straightforward endeavour and it has posed many difficulties in the past.

The present work was driven by the motivation to look into the electrical aircraft concepts that include BESS and make use of the unlimited solar energy by converting it into electricity through solar cells. So far, solar powered aircrafts are mostly designed for low-altitude high-endurance (LALE) applications (see Xinhua et al. (2020)). To the best of the authors knowledge, an adaptive droop controller to guarantee tight voltage regulation and SOC-based power sharing with an overcurrent protection has never been proposed before.

1.1 Main contributions

The novel contribution proposed in this work is twofold:

- First, we propose a unified approach that incorporates an adaptive droop controller for the BESS, based on the instantaneous state of charge of individual units, into the nonlinear sl-PID structure to ensure voltage regulation, accurate power sharing with an inherent overcurrent protection. The developed approach relies on nonlinear systems theory, where an ultimate bound can be found for the input current.
- Numerical simulations are carried out by incorporating actual global horizontal irradiance (GHI) profiles for the photovoltaic (PV) arrays placed on the aircraft wings. The controller performance is verified considering a full testing scenario, that aims to replicate the effects of in-flight actions onto the onboard EPS, such as changes into the flight altitude, or a change in the number of instrumentation components employed.

This nonlinear scheme adopts the droop methodology, and acts regardless of the system and load parameters. Moreover, it can be deployed for both unidirectional and bidirectional DC/DC boost converters in hybrid electric aircraft applications.

1.2 Preliminaries

Consider the following proposition that introduces the nonlinear sl-PID controller.

Proposition 1. Let the output of the nonlinear state-limiting PID (sl-PID) controller, equal to the control input u_i of a plant, be calculated as

$$u_i = -k_{P,i}x_i + M_i \int k_{I,i}\left(r_i - h_i\left(x_i\right)\right) cos\left(\sigma_i\right) - k_{D,i}\frac{\partial h_i}{\partial x_i}\dot{x}_i$$

where $M_i, k_{P.i}, k_{I,i} > 0$, $k_{D,i} \geq 0$.

For a typical zero initial condition of the integral state σ_i, i.e. $\sigma_i\left(0\right) = 0$, the controller state remains within interval

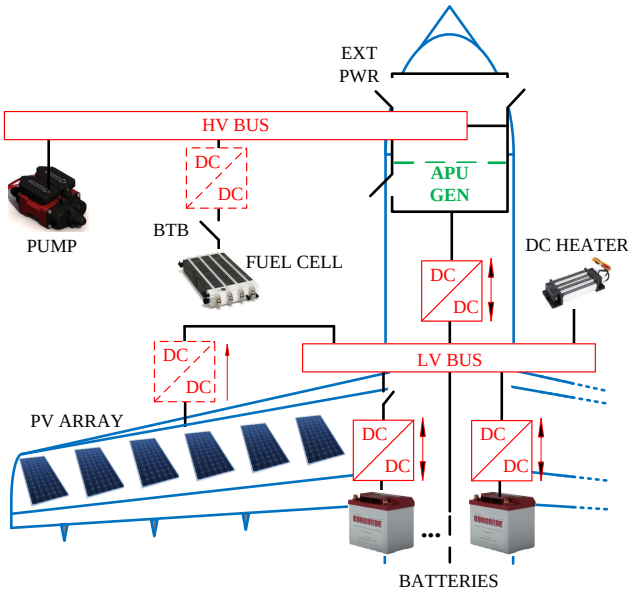

Fig. 1. Typical configuration of an on-board DC MG of a hybrid electric aircraft

$\sigma_i\left(t\right) \in \left[-\frac{\pi}{2}, \frac{\pi}{2}\right]$, $\forall t \geq 0$. Whenever $\sigma_i\left(t\right) \to \pm\frac{\pi}{2}$, then $\dot{\sigma}_i \to 0$, meaning σ_i will converge to the upper or lower limit $\left(\pm\frac{\pi}{2}\right)$ independently of the term $r_i - h\left(x_i\right)$.

Proof. Based on the sl-PID properties developed in Konstantopoulos and Baldivieso-Monasterios (2019).

2. DC MICROGRID MODEL AND CONFIGURATION

A typical configuration of the DC distribution system in a hybrid electric aircraft is shown in Fig. 1. It consists of a high-voltage (HV) and a low-voltage (LV) bus, interconnected via a bidirectional converter to allow two-way power flow. At each bus, one can see various energy sources and batteries connected in parallel with respective loads.

The electrical schematic diagram of the two bus network configuration is presented in Fig. 2. The batteries are represented by controllable voltage sources U and interfaced by bidirectional DC/DC boost converters to the LV bus. At the input of each converter, L and r_s represent the inductor and parasitic resistance, while C and g are the output capacitor and the cable/ line conductance, respectively. The constant power load at the LV bus appears as a current source denoted i_{CPL}, same as the current drawn from the PV array as a function of the irradiance, denoted as $i_{PV} = f(GHI)$.

By applying Kirchhoff's laws one can write the governing dynamics of the converter network in Fig. 2, first at the low-voltage bus, as

$$L_i\frac{di_{L,i}}{dt} = U_i - r_{s,i}i_{L,i} - \left(1 - u_i\right)V_i \tag{1a}$$

$$C_i\frac{dV_i}{dt} = \left(1 - u_i\right)i_{L,i} - i_i \tag{1b}$$

with $i \in \{1, \ldots, n\}$, where $i_{L,i}$, V_i and i_i are the inductor current, and output voltage and current, respectively. The term u_i represents the duty-ratio, bounded within the closed set $u_i \in [0, 1]$.

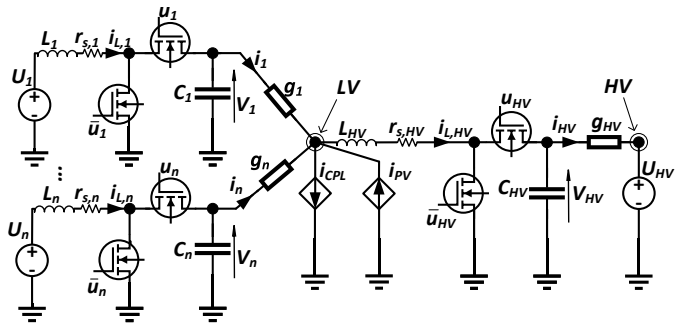

Fig. 2. Schematic diagram of the onboard DC MG of a hybrid electric aircraft

For the converter that connects the two low and high voltage buses, one would similarly get

$$L_{HV}\frac{di_{L,HV}}{dt} = V_{LV} - r_{s,HV}i_{L,HV} - (1-u_{HV})\,U_{HV} \quad (2a)$$

$$C_{HV}\frac{dV_{HV}}{dt} = (1-u_{HV})\,i_{L,HV} - i_{HV}. \quad (2b)$$

where $i_{L,HV}$, V_{HV} and i_{HV} are the input current, and output voltage and current, respectively, of the interconnection converter; u_{HV} is the corresponding duty-ratio.

2.1 Constant power loads

A few remarks will be made here on the CPL model supplied by the LV bus. The constant power load expression is rendered by the power flow equation, that is

$$i_{CPL}V_{LV} = P \quad (3)$$

with P being constant and representing the CPL power. Note that the CPL current i_{CPL} equals the sum of all currents at the LV bus, as follows

$$i_{CPL} = i_{PV} + i_{HV} + \sum_{i=1}^{n} i_i = i_{PV} + i_{HV} + \sum_{i=1}^{n} g_i(V_i - V_{LV}). \quad (4)$$

The voltage solutions V_{LV} when having CPLs are widely known, with the higher voltage solution being the feasible choice. More details on the existence and uniqueness of the feasible solution can be found in Liu et al. (2022).

3. CONTROL DESIGN

A unified approach that incorporates the adaptive droop control into the nonlinear sl-PI framework is being proposed in this section.

3.1 Adaptive droop control

A decentralised control strategy to achieve voltage regulation at each voltage bus, and power sharing among sources in parallel without communication, is the droop-based approach. The conventional droop control in dynamic form can be written as

$$\tau_j\dot{V}_j = V_j^* - V_j - m_j i_j, \quad (5)$$

with $j = \{1, \ldots, n, HV\}$, where i_j is the output current of each converter, V_j^* is a reference voltage value, τ_j a time-constant, and m_j is in general a positive droop coefficient. Since conventional droop control performs poorly when each converter introduces a different output impedance, a common method is to use the robust droop strategy. By considering converters interfacing BESS, the robust droop expression takes the following form

$$\tau_i\dot{V}_i = V^* - V_{LV} - \frac{m_i}{SOC_i^\rho}i_i, \quad (6)$$

where the SOC_i represents the state of charge of the i-th battery, ρ is a positive constant in the natural set, i.e. $\rho \in \mathbb{N}$, and m_i corresponds to the battery capacity.

At the steady state, the following identity takes place

$$\frac{m_1}{SOC_1^\rho}i_1 = \frac{m_2}{SOC_2^\rho}i_2 = \cdots = \frac{m_n}{SOC_n^\rho}i_n. \quad (7)$$

Moreover, if for instance, one assumes same power capacity for each BESS, i.e. $m_1 = m_2 = \cdots = m_n$, the power sharing would be achieved proportional to their current state of charge

$$\frac{1}{SOC_1^\rho}i_1 = \frac{1}{SOC_2^\rho}i_2 = \cdots = \frac{1}{SOC_n^\rho}i_n, \quad (8)$$

with the end goal being that the battery with the highest state of charge would inject more power into the network. Note, however, that when batteries reach the same state of charge, they would inject the same amount of power into the system. A similar behaviour is expected when they are on a charging cycle.

For the converter that connects the two buses, the droop expression takes the following form

$$\tau\dot{V}_{HV} = V^* - V_{LV} - m\,(i_{HV} - i_{set}), \quad (9)$$

with i_{set} being a current reference that sets the amount of current pushed from the high-voltage bus to the low-voltage bus. When $i_{set} < 0$, the power changes direction from low-voltage bus to high-voltage bus.

Remark 1. (Suppressing circulating currents). Droop controllers introduce voltage mismatches, which in turn cause inaccuracies in the current sharing. This difference passes from one converter to other converters, a phenomenon refered to as *circulating currents between converters* (Ghanbari and Bhattacharya, 2020). Avoiding this from taking place is a key feature in parallel operated sources. If one considers for instance two BESS at the LV bus, the circulating current i_{cc} is defined as

$$i_{cc} = i_1 - \frac{m_2}{SOC_2^\rho}\left(\frac{m_1}{SOC_1^\rho}\right)^{-1} i_2. \quad (10)$$

Notice, however, that since a robust droop-based approach has been used and equality (7) holds, then eventually the circulating currant tends to zero, i.e. $i_{cc} \to 0$,

3.2 Voltage reference selection to avoid voltage collapse

Since increasing the power of the CPL causes a potential drop in the CPL voltage V_{LV}, the current will increase to satisfy the power demand. If the system does not have proper control in place to prevent the voltage going below the voltage value of the stable point, then it will continue to drop until zero. Meanwhile, the current will go to infinity. That is, the CPLs impose a power conditioning at the load side, since the nonlinearity introduced into the power balance dynamics could result in voltage collapse (Simpson-Porco et al., 2016) when the requested power increases above a certain level. Therefore, the existence of a steady-state behaviour, in the form of CPLs' voltage

equilibria is critical for the safe and reliable operation of DC microgrids.

A condition for selecting the voltage reference V^* could be put in place to avoid voltage collapse. Several have been proposed in the literature (see for instance Braitor and Konstantopoulos (2022)). Most follow a common idea, around an inequality as shown below

$$V^* > \phi\left(P\right),$$

which in general terms conditions the reference voltage to a value greater than a function $\phi\left(\cdot\right)$ dependent on the CPL power P.

3.3 Adaptive droop-based control with overcurrent capability

Consider the duty ratio as the control input defined as

$$u_j = 1 - \frac{U_j - E_{max,j} sin\left(\sigma_j\right) + r_{v,j} i_{L,j}}{V_j} \tag{11}$$

where σ_j is set to follow the nonlinear dynamics

$$\dot{\sigma}_j = \frac{k_{I,j}}{r_{v,j}} f(i_{L,j}, V_j)\, cos\left(\sigma_j\right) \tag{12}$$

which represents the state-limiting nonlinear PID presented in Proposition 1. Note that function $f\left(\cdot\right)$ takes the following expressions corresponding to the converter interfaced units, i.e.

$$f(i_{L,j}, V_j) = \begin{cases} eqn.\,(6), & \forall\ i \in \{1, \ldots, n\} \\ eqn.\,(9), & HV\ interconnection \end{cases} \tag{13}$$

Assumption 1. The present approach considers at least one converter-interfaced source connected to the low-voltage bus to stabilise the bus voltage.

Note that the previous assumption is a sensible and not a restrictive one, particularly in case of islanded microgrids, which is also the case of the self-contained onboard aircraft DC EPS considered herein.

Next, by replacing the control input u_i from (11) into the open-loop current dynamics (1a), one obtains the following closed-loop current dynamics

$$L_j \frac{di_{L,j}}{dt} = E_{max,j} sin\left(\sigma_j\right) - \left(r_{s,j} + r_{v,j}\right) i_{L.j} \tag{14}$$

where one can see that $E_{max,j} sin\left(\sigma_j\right)$ represents a virtual voltage, and $r_{v,j}$ a virtual resistance in series with the parasitic resistance $r_{s,j}$. Given that the value of the parasitic resistance is negligible compared to the virtual resistance (i.e. $r_{s.j} << r_{v,j}$), at steady state there is

$$i_{L,j} \approx \frac{E_j sin\left(\sigma_j\right)}{r_{v,j}}. \tag{15}$$

Consider the following proposition that guarantees current limitation.

Proposition 2. The solution $i_{L,j}\left(t\right)$ of (14) with the initial condition $i_{L,j}\left(0\right) \leq \frac{E_{max.j}}{r_{v,j}}$ is uniformly ultimately bounded, i.e. $|i_{L,j}\left(t\right)| < i_{L,i}^{max}, \forall t \geq 0$, with the maximum current given as $i_{L,j}^{max} = \frac{E_{max.j}}{r_{v,j}}$.

Proof. Consider the following continuously differentiable Lyaponov function candidate

$$W_j = \frac{1}{2} L_j i_{L,j}^2 \tag{16}$$

The time derivative of W yields

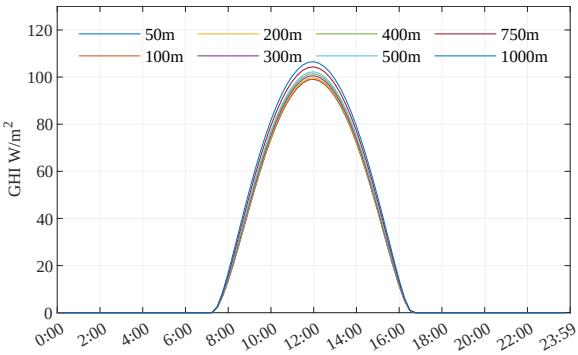

Fig. 3. 24-hour GHI profiles on a sunny spring day at different altitude levels

$$\begin{aligned} \dot{W}_j = L_j i_{L,j} \dot{i}_{L,j} &= -\left(r_{s,j} + r_{v,j}\right) i_{L,j}^2 + E_{max,j} sin\left(\sigma_j\right) i_{L,j} \\ &\leq -\left(r_{s,j} + r_{v,j}\right) i_{L,j}^2 + |E_{max,j} sin\left(\sigma_j\right)|\, |i_{L,j}|. \end{aligned} \tag{17}$$

Provided the bounded state $\sigma_j \in \left[-\frac{\pi}{2}, \frac{\pi}{2}\right]$ from the nonlinear sl-PID design, one has

$$\dot{W}_j \leq -\left(r_{s,j} + r_{v,j}\right) |i_{L,j}|^2 + E_{max,j}\, |i_{L,j}|, \tag{18}$$

which implies that

$$\dot{W}_j \leq -r_{s,j} i_{L,j}^2, \forall\, |i_{L,j}| \geq \frac{E_{max}}{r_{v,j}}. \tag{19}$$

By virtue of (19), the solution $i_{L,j}\left(t\right)$ is uniformly ultimately bounded. Therefore, if initially $|i_{L,j}\left(0\right)| \leq \frac{E_{max,j}}{r_{v,j}}$, then it holds that

$$|i_{L,j}\left(t\right)| \leq \frac{E_{max,j}}{r_{v,j}}, \forall t > 0, \tag{20}$$

due to invariant set property. Based on the desired overcurrent protection, it should hold true that

$$|i_{L,j}\left(t\right)| \leq i_{L,j}^{max}, \forall t > 0, \tag{21}$$

for a given maximum value of $i_{L,j}^{max}$ of the inductor current. By substituting (20) into (21), one can clearly select the parameters $E_{max,j}$ and $r_{v,j}$ in the proposed controller in order to satisfy

$$r_{v,j} i_{L,j}^{max} = E_{max,j}. \tag{22}$$

The proof is complete. □

Notice that any selection of the positive constants $E_{max,j}$ and $r_{v,j}$ that satisfy equation (22) results in the desired overcurrent protection (21). That is, an upper limit for the converter inductor current is ensured regardless of the load magnitude or system parameters.

Remark 2. (Bidirectional overcurrent protection). From the closed-loop dynamics (14) and controller dynamics (12), one has $f\left(i_{L,j}, V_j\right) = 0$, then $\sigma_j = \sigma_{j,e}$, while the value of the inductor current becomes

$$i_{L,je} = \frac{E_{max,j} sin\left(\sigma_{j,e}\right)}{r_{v,j}}. \tag{23}$$

Nevertheless, since $\sigma_{j,e} \in \left[-\frac{\pi}{2}, \frac{\pi}{2}\right]$, then the inductor current can be both positive and negative, thus, ensuring the bidirectional operation of the bidirectional converter. When $\sigma_{j,e} = -\frac{\pi}{2}$, then $i_{L,je} = -\frac{E_{max,j}}{r_{v,j}} = -i_{L,j}^{max}$ that corresponds to the overcurrent protection in both directions of the power flow.

Note that since the proposed controller slows down near the imposed limits, it does not suffer from integrator wind-up which may introduce instability into the system.

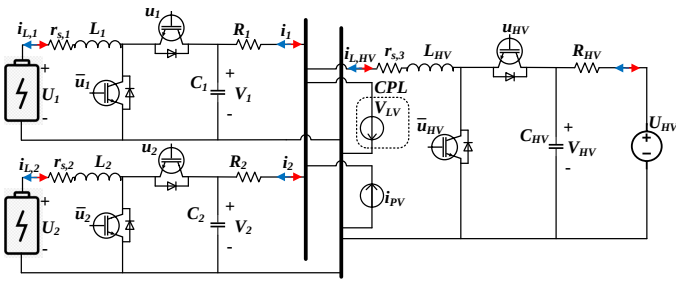

Fig. 4. Schematic diagram of the MG considered for simulation testing

4. SIMULATION RESULTS

The proposed aicraft EPS concept includes PV arrays arranged onto the aircraft wings injecting power at the LV bus. The amount of irradiance panels receive intuitively depends also on the aircraft altitude. With the assistance of the Solar radiation Data (SoDa) database and HelioClim archives, for a location in Central Europe, one can note that the GHI value changes proportionally with the increase in altitude. See for instance, in Fig. 3, that as expected, the higher the altitude level the larger the GHI value. For simulation purposes. converting GHI to electrical power (or electrical current) may be done with mathematical formulae similar to the ones reported in Duffie and Beckman (2013).

The MG under consideration is presented in Fig. 4 with the parameters shown in Table 1. The aim is to test the controller performance and behaviour when required to deliver the following tasks: maintain the voltage at the LV bus close to the reference $V^* = 540\,V$, share the power among the BESS proportionally to their state of charge, guarantee an upper bound for the input current of each converter unit. Notice that by employing the proposed control approach onto the EPS, one could attain additional objectives in the electrification process such as i) reduced subsystems weight and volume; ii) improved reliability and maintainability; ii) minimised environmental impact; iii) improved modularity and EPS efficiency; iv) new capabilities and cost effective rapid technology insertion.

The simulation results have been illustrated in Fig. 5 considering a full testing scenario as follows. Batteries start with an initial state-of-charge of 89%, and 75% respectively. During the first $20\,s$, both batteries and PV are supplying the CPL at the LV bus. Moreover, power is being received at the LV bus from the HV bus (see in Fig. 5c). In Fig. 5a, one can notice that battery 1 gives more power than battery 2 since it has a higher SOC.

Table 1. System and control parameters

System and control parameters	Values
$R_1,\ R_2,\ R_{HV}$	$0.04\,\Omega,\ 0.12\,\Omega,\ 0.1\,\Omega$
$L_1,\ L_2,\ L_{HV}$	$0.002\,H$
$r_{s,1},\ r_{s,2},\ r_{s,3}$	$0.001\,\Omega$
$U_{BAT,1},\ U_{BAT,2}$	$48\,V$
$C_1,\ C_2,\ C_{HV}$	$100\,\mu F$
ρ	3
$k_{I1},\ k_{I2},\ k_{I3} \times 10^{-4}$	1.1, 6, 9
$i_{max,1},\ i_{max,2},\ i_{max,3}$	$10\,A,\ 10\,A,\ 5\,A$
$r_{v,1},\ r_{v,2},\ r_{v,3}$	$1\,\Omega$

According to the developed theory, the difference between the SOCs is expected to become null in finite time, i.e. $\Delta SoC \to 0$. The voltages are closely regulated to the reference value V^* (Fig. 5b).

Next, at $t = 20\,s$, the injected PV power increases as shown in Fig. 5c, i_{PV} goes up possibly caused by an increase in aircraft altitude. Both battery currents and the current received from the HV bus decrease, while the voltage returns to its close to reference value (Fig. 5c), following a short transient. All currents remain below their maximum limit specified in Table 1.

The power requested at the LV bus increases by 5%, at $t = 40\,s$, associated with a rise in instrumentation components used onboard. To cope with the new requested load, the HV bus and batteries start pushing more power as observed in Fig. 5a. In Fig. 5b, following a short transient with a a 15% undershoot, the voltages recover to their initial value close to V^*.

Finally, at $t = 60\,s$, parameter i_{set} corresponding to the converter interconnecting the two buses slowly decreases, thus, reducing the power to the LV bus. Then, both batteries start ramping up their respective injected power (Fig. 5a). The voltages drop slightly to below V^* (Fig. 5b).

Throughout the entire simulation, the difference in SOCs between the two batteries was decreasing, eventually becoming null when batteries reach the same SOC. The convergence rate to zero can be adjusted using the control parameter ρ. Note also that the input currents remain at all times below their maximum limit specified in Table 1.

5. CONCLUSION

An adaptive droop-based strategy with an overcurrent protection has been implemented for ESS in onboard DC MGs for hybrid electric aircrafts. The proposed methodology uses nonlinear systems theory, to analytically guarantee an ultimate bound for current, and to ensure tight voltage regulation, and power sharing. Simulation testing has been carried out for an onboard DC EPS with two LV and HV buses, incorporating BESS, PV arrays and CPL displaying a normal operation with tight voltage regulation and accurate load power distribution, while maintaining an upper current bound at all times. These advances in EPS control design are vital prerequisites for the electrification trend to continue as they will lead to lower fuel consumption, lower emissions and reduced overall costs.

REFERENCES

Baidya, S. and Nandi, C. (2022). A comprehensive review on dc microgrid protection schemes. *Electric Power Systems Research*, 210, 108051.

Behera, M., Saikia, L., Ramoji, S., Dekaraja, B., and Bhagat, S. (2022). A novel decentralized FO voltage and current control scheme for voltage and frequency regulation in inverter dominated islanded microgrids using improved droop control. *IFAC-PapersOnLine*, 55(1), 679–684.

Braitor, A.C., Konstantopoulos, G., and Kadirkamanathan, V. (2020). Admittance matrix computation and stability analysis of droop controlled DC micro-

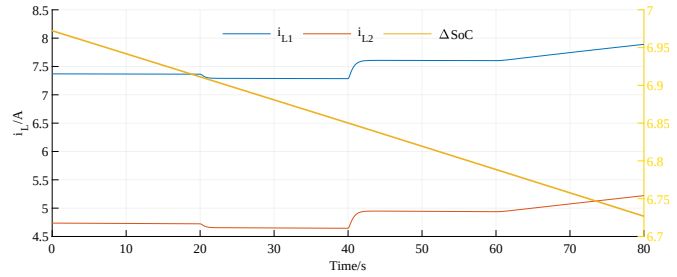

a) battery currents and state-of-charge difference

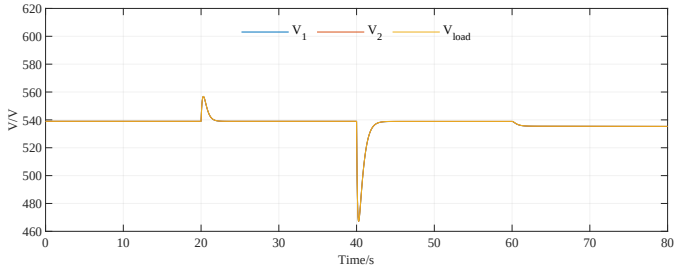

b) capacitor and LV bus voltages

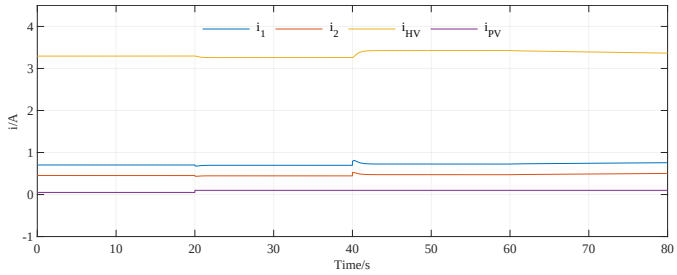

c) output currents

Fig. 5. Dynamic response of the system states

grids with CPL. *IFAC-PapersOnLine*, 53(2), 13525–13530. 21th IFAC World Congress.

Braitor, A.C., Mills, A., Kadirkamanathan, V., Konstantopoulos, G., Norman, P., and Jones, C. (2018). Control of dc power distribution system of a hybrid electric aircraft with inherent overcurrent protection. In *2018 IEEE International Conference on Electrical Systems for Aircraft, Railway, Ship Propulsion and Road Vehicles and International Transportation Electrification Conference*, 1–6.

Braitor, A.C. and Konstantopoulos, G.C. (2022). On the existence and uniqueness of equilibria in meshed dc microgrids with cpls. In *2022 30th Mediterranean Conference on Control and Automation (MED)*, 1030–1035.

Cingoz, F., Elrayyah, A., and Sozer, Y. (2017). Plug-and-play nonlinear droop construction scheme to optimize islanded microgrid operations. *IEEE Transactions on Power Electronics*, 32(4), 2743–2756.

Duffie, J.A. and Beckman, W.A. (2013). *System Thermal Calculations*, chapter 10, 422–446. John Wiley and Sons, Ltd.

Ferahtia, S., Djerioui, A., Rezk, H., Chouder, A., Houari, A., and Machmoum, M. (2022). Adaptive droop based control strategy for dc microgrid including multiple batteries energy storage systems. *Journal of Energy Storage*, 48, 103983.

Gaynor, G.H. (2015). *Boeing and the 787 Dreamliner*, 187–218.

Ghanbari, N. and Bhattacharya, S. (2020). Suppressing circulating currents of battery management systems in droop based microgrids. In *2020 IEEE Transportation Electrification Conference and Expo (ITEC)*, 871–876.

Guerrero, J.M., Vasquez, J.C., Matas, J., de Vicuna, L.G., and Castilla, M. (2011). Hierarchical control of droop-controlled ac and dc microgrids 2014;a general approach toward standardization. *IEEE Transactions on Industrial Electronics*, 58(1), 158–172.

Huang, P.H., Liu, P.C., Xiao, W., and Moursi, M.S.E. (2015). A novel droop-based average voltage sharing control strategy for DC microgrids. *IEEE Transactions on Smart Grid*, 6(3), 1096–1106.

Jin, X., Shen, Y., and Zhou, Q. (2022). A systematic review of robust control strategies in dc microgrids. *The Electricity Journal*, 35(5), 107125.

Konstantopoulos, G.C. and Zhong, Q. (2019). Current-limiting dc/dc power converters. *IEEE Transactions on Control Systems Technology*, 27(2), 855–863.

Konstantopoulos, G.C. and Baldivieso-Monasterios, P.R. (2019). State-limiting PID controller for a class of nonlinear systems with constant uncertainties. *International Journal of Robust and Nonlinear Control*.

Liu, Z., Su, M., Sun, Y., Han, H., Hou, X., and Guerrero, J.M. (2018). Stability analysis of dc microgrids with constant power load under distributed control methods. *Automatica*, 90, 62 – 72.

Liu, Z., Su, M., Sun, Y., Zhang, X., Liang, X., and Zheng, M. (2022). A comprehensive study on the existence and stability of equilibria of dc-distribution networks with constant power loads. *IEEE Transactions on Automatic Control*, 67(4), 1988–1995.

Mohamed, Y.A.I. and El-Saadany, E.F. (2008). Adaptive decentralized droop controller to preserve power sharing stability of paralleled inverters in distributed generation microgrids. *IEEE Transactions on Power Electronics*, 23(6), 2806–2816.

Roboam, X., Sareni, B., and Andrade, A.D. (2012). More electricity in the air: Toward optimized electrical networks embedded in more-electrical aircraft. *IEEE Industrial Electronics Magazine*, 6(4), 6–17.

Simpson-Porco, J.W., Dörfler, F., and Bullo, F. (2017). Voltage stabilization in microgrids via quadratic droop control. *IEEE Transactions on Automatic Control*, 62(3), 1239–1253.

Simpson-Porco, J.W., Dörfler, F., and Bullo, F. (2016). Voltage collapse in complex power grids. *Nature Communications*, 7(1), 10790.

Steinbauer, T., Leiprecht, G., and Havranek, W. (2004). High performance hil real time for the airbus a380 electrical backup hydraulic actuators. In *2004 Mini Symposia UKACC Control*, 71–74.

Wheeler, P. and Bozhko, S. (2014). The more electric aircraft: Technology and challenges. *IEEE Electrification Magazine*, 2(4), 6–12.

Xinhua, L., Kaijun, S., and Feng, L. (2020). General optimal design of solar-powered unmanned aerial vehicle for priority considering propulsion system. *Chinese Journal of Aeronautics*, 33(8), 2176–2188.

Zhang, X., Yang, X., Han, Y., Yang, P., and Zalhaf, A.S. (2022). Consensus enhanced droop control strategy for islanding mode multi converter system. *Energy Reports*, 8, 301–309.